



STUDIES OF DANSGAARD-OESCHGER CLIMATE EVENTS FROM GREENLAND ICE CORES

BACHELOR THESIS

Written by *Anna Maria Klüssendorf*
January 22, 2021

Supervised by
Dorthe Dahl-Jensen

UNIVERSITY OF COPENHAGEN



UNIVERSITY OF
COPENHAGEN

NAME OF INSTITUTE: Niels Bohr Institute

NAME OF DEPARTMENT: Physics of Ice, Climate and Earth

AUTHOR(S): Anna Maria Klüssendorf

EMAIL: ncd822@alumni.ku.dk

TITLE AND SUBTITLE: Studies Of Dansgaard-Oeschger Climate Events From
Greenland Ice Cores
-

SUPERVISOR(S): Dorte Dahl-Jensen

HANDED IN: 15th January 2020

DEFENDED: 24th January 2020

NAME _____

SIGNATURE _____

DATE _____

Abstract

Analyses of Greenland ice cores are an important approach in order to reconstruct the climate. A continuous flow analysis furnishes high resolution data of the chemical composition of the ice. Annual signals in the dust and conductivity record are used to determine the annual layer thickness of the DYE-3 ice core of the Holocene. The accumulation rate for the drilling sites GRIP, GISP2, NEEM and NGRIP has been calculated applying the Dansgaard-Johnsen flow model to age and depth data. By comparing the accumulation rate to the stable water isotope record, an intimate correlation between the accumulation rate and the temperature was ascertained. The relation between the change of the two parameters can be seen as linear and applicable to all the drilling sites investigated. However, a site-specific variation of the change in $\delta^{18}\text{O}$ compared to the present average value has been observed. This indicates a changing shape of the Greenlandic ice sheet. Using a $\delta^{18}\text{O}$ -height relationship calibrated for the current climate period, a decline of the ice sheet after the onset of the Holocene can be considered. During the glacial period, the locations of the current drilling sites NGRIP and NEEM are expected to have been respectively 300m and 600m more elevated than today.

Contents

1	Introduction	3
2	Scientific Background	4
2.1	Ice Flow and Thinning	4
2.2	Densification	4
2.2.1	Density Correction	5
2.3	Stable Water Isotopes	6
2.3.1	Isotopic Ratio and the δ Notation	6
2.3.2	Isotopic Fractionation	7
3	Ice Core Dating Methods	7
3.1	Stable Water Isotope Record	7
3.2	Ice Core Impurities	8
3.3	Continuous Flow Analysis	8
3.3.1	DYE-3 Measurement	10
3.4	Annual Layer Counting	11
3.5	Dansgaard-Johnsen Model	12
4	Accumulation Rate	14
4.1	Accumulation Rate and Stable Water Isotopes	14
4.2	Sensitivity of the Accumulation Rate to Changes in $\delta^{18}\text{O}$	15
5	Investigation of the Dansgaard-Oeschger Events	17
5.1	Relative Changes in Accumulation Rate and $\delta^{18}\text{O}$	18
5.2	Correlation to Elevation Changes	19
6	Conclusion	20
7	References	21

1 Introduction

In the past few decades, climate change has become an important issue in science as well as society. The global temperatures have increased, leading to a rise in the global sea level. According to measurements carried out by NASA, the current rate of change in sea level is 3.3 mm yr^{-1} [1]. As a result of global warming, melting continental glaciers and ice sheets are the most significant contributors. The Greenland ice sheet contains the second largest mass of ice in the world and contributes to the rising sea level by almost 30% [2]. During the Last Glacial Maximum, the temperatures are believed to have been on average 25°C less than at present and the volume of the Greenlandic ice sheet about 40% higher. This corresponds to a sea level around 120 m lower than today [3]. However, the glacial period, covering a time interval from 119.1 ka to 11.7 ka before present, shows a highly fluctuating climate signal, in which the cold glacial climate is interrupted by milder periods. The phases with higher temperatures are referred to as *interstadials*, and the corresponding periods of full glacial conditions are known as *stadials* [4]. These fluctuations can be seen in abrupt shifts of the stable water isotope ratio, which are referred to as *Dansgaard-Oeschger (DO) Events*. Figure 1 shows 20 of the 25 known DO Events in a stable isotope record from GISP2.

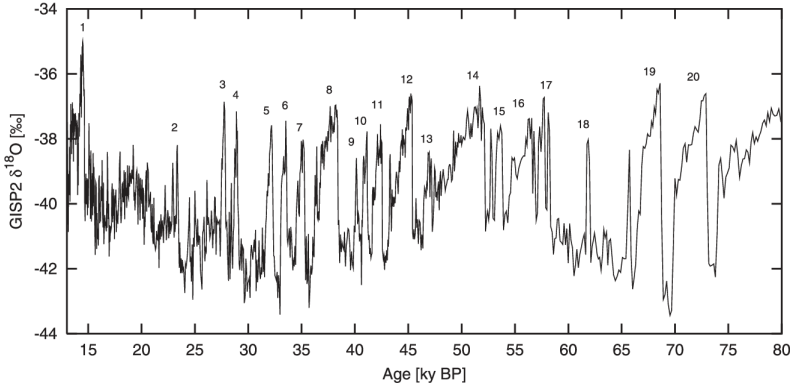


Figure 1: Plot of the stable water isotope record of the ice core drilled at GISP2 as a function of its age in ka in a period from 80ka to 12ka years before present. The numbers are indicating the occurring Dansgaard-Oeschger Events in this time interval. Taken from H. Braun (2009) [5].

The duration of a single event usually lasts only a few decades and the measured temperatures fluctuate between 8°C and 16°C . These changes are presumably caused by the atmospheric and oceanic circulation. Warm DO events occurred when the thermohaline circulation was strong, transporting heat polewards thus warming the water and atmosphere around Greenland. Cold conditions are likely a result of a drop in the heat transport. The changing strength of the oceanic circulation can not yet be explained [4].

Ice caps can be seen as sensitive archives for previous climate conditions. Atmospheric air gets trapped into air bubbles near the surface of the ice sheet and are then advected downwards as new precipitation is accumulating. This provides a record for the past atmospheric composition. The abundant stable water isotopes preserved in the ice itself can be linked to the local temperature at time of precipitation. Therefore, they reveal a seasonal variation which can be found as an annual signal in the ice core. A compilation of an accurate ice chronology, assigning the age to the depth of the ice, is essential in order to interpret the ice core records properly. By analysing the chemical composition and impurities in the ice, annual layers can

be detected. Annual layer counting is one of the most important dating methods in ice and climate research. Data of the chemical composition are collected in high resolution using a system for *Continuous Flow Analysis*. In this thesis remeasured data from the DYE-3 ice core are processed in order to determine the annual layer thickness of this ice core. Furthermore, the relationship between the stable water isotopes and the accumulation is studied, using the ice core data from different drilling sites in Greenland. The same data support an investigation of the geographically varying climate fluctuations.

2 Scientific Background

2.1 Ice Flow and Thinning

An ice sheet can be considered a dynamic body constantly undergoing the flowing and deforming of the ice. In the accumulation zone in the central part of the ice sheet, snow is continuously accumulated, burying the previous layers with time. Since snow is a quasi-viscous material, it deforms under the applied stress of the overlying layers. The general ice flow downwards and towards the margins thins the annual layers gradually and causes the convex shape of an ice sheet. This is illustrated in Figure 2. An ice core record is ideally carried out close to the ice divide, as here the horizontal flow is slow and thereby negligible. Thus, the ice originates from approximately the same location near the ice divide at a certain depth.

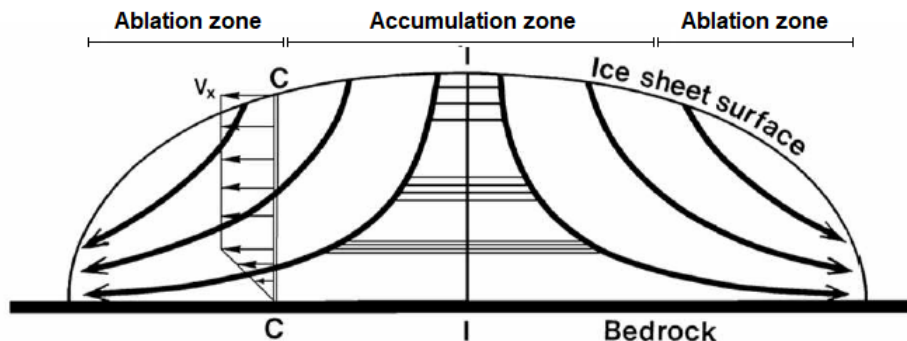


Figure 2: Idealised illustration of the ice flow, indicated by the thick arrows, through the cross section of a large glacier. The horizontal line around the ice divide, I , represent annual layers, which get stretched and thinned with depth. C marks an arbitrary position on the ice sheet and V_x is the horizontal velocity trough the ice cap. Taken from Bizet, B. J. R. (2006) [6].

2.2 Densification

When new snow gets deposited on a Greenland ice sheet it has a density of $50\text{-}70 \text{ kg m}^{-3}$. If the temperature stays at freezing temperatures, no melting occurs and new layers of snow bury the old ones. The overlying weight compresses the snow gradually. When a density of about 400 kg m^{-3} is reached, the snow is in an intermediate state of transformation, in which the air is still in contact with the atmosphere. This porous material is called firn and gets compacted due to rearrangement and growth of grains until it reaches a critical density of $\rho_c = 550 \text{ kg m}^{-3}$. Through plastic and elastic deformation at the interface between the grains the density increases further. At a depth of about 80 m all the pores between the grains are

sealed off, creating closed air bubbles. The density is increased to 830 kg m^{-3} and the firn has transformed to ice at about 150 m depth. The depth scale of the transition can be seen in Figure 3. With increasing depth, the closed air bubbles get compressed and the density can increase to a maximum of 917 kg m^{-3} , which is the density of pure glacial ice. After this, it is not possible to compress the ice any further and layer thinning only occurs due to plastic deformation and ice flow.

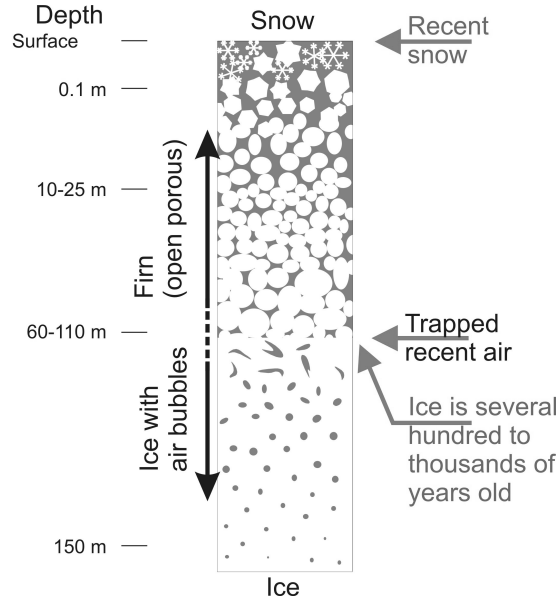


Figure 3: Schematic illustration of the transformation of snow to ice in an ice sheet on a depth scale. The different stages of transformation are indicated. Taken from *The firn zone: Transforming snow to ice* [7].

These three stages of snow deformation were described by Herron and Langway, who introduced an empirical based model to describe the densification rate, depending on the surface temperature, T , and the overburden pressure, which is determined by the accumulation rate, A . The density is increasing exponentially with depth, as can be seen from Equation 1, an empirical based relation [8].

$$\rho(z) = \rho_i - (\rho_i - \rho_o) \exp -Cz \quad (1)$$

Here ρ denotes the density at depth, z , and ρ_o the density of the snow on the surface of the ice. The constant, C , is related to the temperature and the transition depth of firn and has to be tuned for each drilling site.

2.2.1 Density Correction

A drilled ice core used for analysis contains both ice and firn. The density variation, described in Section 2.2, has to be accounted for when using flow models. Since the firn layer only covers the upper 100 meters of an ice core of around 3000 m length, as can be seen in Figure 3, an approximation can be made, where it is assumed that all firn is compressed to ice. This reduces the total ice thickness of the ice sheet due to the fact that all air is removed. For central Greenland the equivalent ice thickness after the density correction is about 25 m less than when snow and firn are included. When analysing the ice cores from the different drilling

sites, the density is assumed to be approximately constant all over Greenland and density data for NEEM is used to correct the density variation. The data contains the density of firn and ice for every 55 cm as well as the depth before and after the correction, showing how much air is removed in each layer of 55 cm thickness, as this varies due to compression of the ice with depth. At a depth of 200 m, when the density has reached $\rho_i = 917 \text{ kg m}^{-3}$, the air correction value is 23.42 m, meaning that this amount of air is removed by compressing the firn to ice. Hence, it has to be subtracted from the total thickness of the ice. In order to construct new data points for the depths and annual layer thickness corresponding to the corrected depths for all the ice cores, the discrete values are connected by interpolation and used for further modelling.

2.3 Stable Water Isotopes

In nature, hydrogen and oxygen, the constituents of water, exist as isotopes. Isotopes of a certain element contain the same number of protons in each atom, but the amount of neutrons differs, resulting in different atomic masses. For oxygen three stable isotopes are known, which occur in different abundances, ^{16}O (99.76%), ^{17}O (0.04%) and ^{18}O (0.2%). The hydrogen atom has two stable isotopes, ^1H (99.984%) and deuterium, ^2H (0.016%) [9].

2.3.1 Isotopic Ratio and the δ Notation

Besides the mass variation they also have different physical properties, like their mobility. This is indicated by the kinetic energy of a molecule:

$$E_{Kin} = \frac{1}{2}m\bar{v}^2 = kT \quad (2)$$

Here m is the mass of the molecule, \bar{v} its average velocity, k the Boltzmann constant and T the temperature. In order to possess the same amount of energy, an isotope with lower mass must have a higher velocity at a certain temperature. This results in faster diffusion and a higher collision frequency and thereby to a higher possibility of reacting. This means that lighter isotopes tend to evaporate faster than heavier ones. This effect causes a phenomenon, known as *isotopic fractionation*, expressed by the *isotopic ratio*, R , which is defined as the ratio between the number of heavy and light isotopes, N_h and N_l , respectively.

$$R = \frac{N_h}{N_l} \quad (3)$$

This ratio usually is a small number due to the small relative amount of the heavier isotope, and is difficult to measure. Therefore, the isotopic composition in ice is described by the δ -value. This quantity denotes the relative deviation of a measured isotopic ratio with respect to a standard, for which mostly the Vienna Standard Mean Ocean Water (VSMOW) is used [10].

$$\delta = \frac{R_{sample}}{R_{VSMOW}} - 1 \quad (4)$$

The δ -value for standard water, $\delta^{18}\text{O}_{VSMOW}$ and $\delta^2\text{H}_{VSMOW}$, is defined to be zero [11]. The $\delta^{18}\text{O}$ rate in Equation 5 describes the reduction of the heavy oxygen isotope, ^{18}O , in relation to the more common and lighter ^{16}O isotope in water molecules in the ice. δ is unitless, but since the ratios vary very little, the value is given in permille.

$$\delta^{18}O_{sample} = \left(\frac{\frac{[^{18}O]}{[^{16}O]}_{sample}}{\frac{[^{18}O]}{[^{16}O]}_{VSMOW}} - 1 \right) \cdot 1000\text{‰} \quad (5)$$

2.3.2 Isotopic Fractionation

The isotopic fractionation process is expressed by the fractionation factor, α . It describes the difference in water vapour pressure between the lighter and the heavier isotopes [10], assuming the water vapour in a body of water or ice to be in equilibrium. It is defined as the fraction of the ratio of condensate, R_c , and the ratio of water vapour, R_v , in a parcel of moist air.

$$\alpha = \frac{R_c}{R_v} \quad \text{and} \quad \delta_c = \alpha(\delta_v + 1) - 1 \quad (6)$$

Here the subscripts c and v represent the condensate and the water vapour, respectively. The fractionation factor depends on the temperature, the isotopic species and the features of the condensate. The condensate is assumed to fall out immediately as precipitation. When the air parcel is floating over an ice sheet, the precipitation is deposited and becomes part of the ice core.

3 Ice Core Dating Methods

Dating ice cores aims to build up an accurate time scale by assigning the depth of the ice to a specific year in time. There are several methods of dating the drilled ice cores. At high accumulation sites the stable water isotope records give a reliable chronicle of the seasonal temperature signals. Soluble compounds reveal an annual tendency and can be measured using chemical analysis. Detecting annual layers in a vertically drilled ice core can be used to reconstruct past accumulation rates by applying a steady state model. Because the accumulation rates are strongly dependent on the surface temperature, a correlation to the oxygen isotopes can be determined. Afterwards, a non-steady state model allows the development of a time scale. Dated global events, such as large forest fires or volcanic eruptions, can be seen in the acidity signal, as they deposit black carbon and ammonium on the ice, effecting the conductivity measurements.

3.1 Stable Water Isotope Record

As stated above, the lighter isotopes have a higher saturation vapour pressure. This implies that after evaporation, the vapour is less rich in heavy isotopes than the original water. The remaining liquid water now has a higher concentration of ^{18}O , the same applies to the condensed vapour. A temperature drop enhances the condensation and increases the amount of lighter isotopes in the water vapour. δ will decrease until deposition on the ice sheet occurs. Consequently, the abundant stable water isotopes preserved in the ice itself can be used as climate proxies as they are correlated to the local temperature at the time of precipitation and therefore reveal a seasonal variation [12]. During winter season with lower temperatures, more water precipitates, resulting in lower δ -values than during summer time with higher temperatures. Under assumption of a uniform deposition of accumulation, an annual signal of varying δ -values can be observed in an ice core.

3.2 Ice Core Impurities

While in the upper part of an ice core, the $\delta^{18}\text{O}$ -signal shows a clear annual signal due to a rather high temperature difference between the seasons, the seasonal variation is reduced during the process of densification further down in the ice. Here, water isotopes can be diffused by moving into the open pores before the close-off. In layers only a few centimetres thick the signal can be obliterated. For low accumulation sites with thin annual layers, impurity measurements can be used as a dating method, since the particles are unaffected by diffusion. Their concentration varies seasonally. For instance, the terrestrial dust signal shows a peak in springtime, because stronger storms during this season transport high amounts of dust to Greenland. Ionised particles influence the conductivity measurements, presenting an annual signal. High values of conductivity can be an indication of volcanic activity. An explosive volcanic eruption releases acids and fragmented lava, called tephra, into the atmosphere. Whereas the heavy pyroclasts deposit near the crater, the finer particles, such as ash and lapilli, rise into higher atmospheric layers and get distributed over broad areas as they get transported by upper winds [13]. Deposited and cemented tephra layers can be found in ice cores. However, more common are layers not containing tephra but elevated level of acids like sulphate or sometimes fluoride, influencing the acidity signal (see Figure 4). By analysing the filtered particles, the volcano of origin can be established. As most volcanic eruptions are dated, they play an important role in constructing an ice core chronology. Greenlandic ice cores are mostly impacted by Icelandic and Alaskan volcanoes, but if the eruption is strong enough to inject particles into the stratosphere, layers originating from volcanoes of the tropics or the Southern hemisphere can be found [14].

3.3 Continuous Flow Analysis

The dating of ice cores is based on the chemistry, the impureness and the isotope concentration, which are observed to follow an annual cycle. In order to measure the chemical composition and establish a time scale *Continuous Flow Analysis (CFA)* is used. A CFA system, developed by the University of Bern, was re-designed and optimised to determine transient signals in thinner layers of deep polar ice cores with high resolution by the Centre for Ice and Climate at the University of Copenhagen. It is able to detect the electrolytic conductivity of the ice core meltwater, as well as the concentration of sodium (Na^+), calcium (Ca^{2+}), hydrogen peroxide (H_2O_2), ammonium (NH_4^+), the content of dust particles and the acidity [15]. Furthermore, the system allows an analysis of the trapped air by separating the air bubbles from the meltwater, and a determination of both gas and water isotopes. The CFA system primarily consists of an ice core sample placed on a melthead in a freezer, valves for both standards and samples, a debubbler and various modules for the analysis of the chemistry contents mentioned above. The apparatus is situated in a laboratory at room temperature. The detailed setup can be seen in Figure 5. The ice sample with dimensions of $34 \times 34 \text{ mm}^2$ in cross section and about 100 cm length is held in a removable Plexiglas frame, which is fastened on a fixed shorter frame of same material and a centring frame above the melthead. The aluminium melthead has a square shape and consists of an outer ring and an inner area with four drain holes by the edges and one drain hole at the centre of drain channels, respectively, separating the contaminated melt water from the surface of the sample. During the analysis, a stable melt rate is important in order to avoid baseline drifts and increased signal noise. This is achieved by setting the melthead to a constant temperature and placing a weight on top of the ice sample, which maintains a constant downward force. A draw-wire attached with a hook to the top of the weight runs along the backside of the frame and registers the melt progress. The melt

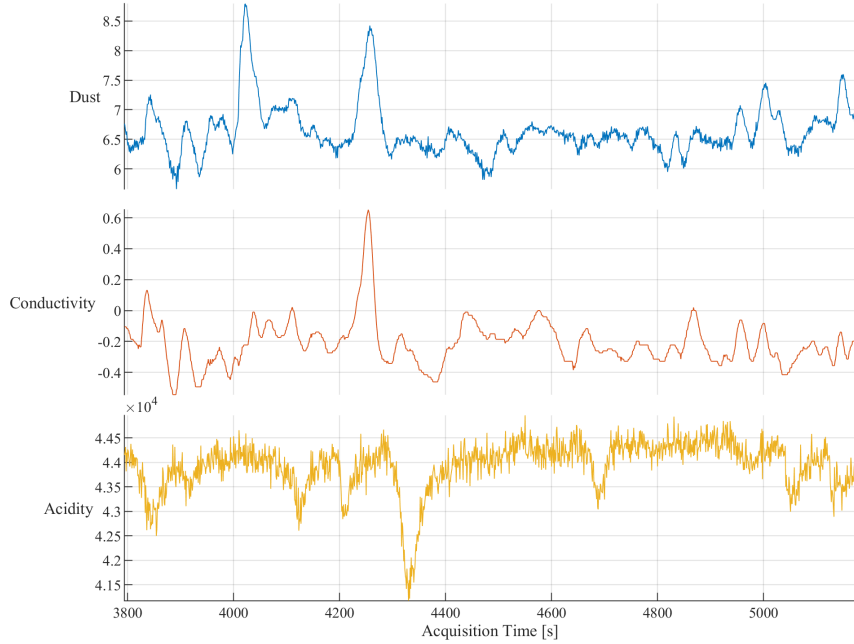


Figure 4: Dust (blue), conductivity (red) and acidity (yellow) record measured in Bag 1741 corresponding to a depth of 1790.5 to 1791.5 m are plotted against the acquisition time on a logarithmic scale. An annual signal can be seen in the dust and conductivity. The distinct peaks in all the 3 records at around 4200 s indicate a volcanic signal, whereas the previous peak in the dust signal is likely due to contamination at a break in the ice sample.

speed is calculated as the wire gets wind on a coil underneath the melthead. Shortly after the melthead a 6-port selection valve is installed, that allows the switching between the sample melt water stream, ultra pure blank water (MilliQ), that is degassed by helium, and standard solutions. By pumping the meltwater through a debubbler, which is hermetically sealed to ambient air, air bubbles get removed from the sample. The debubbler is constituted of an equilateral triangular cell with a side length of 10 mm and a depth of 2 mm. It contains one inlet in the lower left corner for the incoming meltwater sample with a flow of 8ml/min and two outlets; the lower right one for the debubbled meltwater and the upper for the air bubbles and excess meltwater, which is approximately 25% of the sample, respectively [15]. The remaining debubbled meltwater follows the pump tubing to the analytical system, where the chemical composition gets determined. A conductivity meter measures the conductivity, and a particle detector determines concentration and size of non-chemical particles using a laser beam. Bigger particles are absorbed when the meltstream passes a 20 micron (μm) filter for the particle analysis of e.g. tephra layers in order to identify the volcano eruption and thereby be able to date the ice core precisely. A photo-multiplier uses a fluorescence method to ascertain the ammonium concentration, whereas an absorption method is used to measure the concentration of sodium, using a light diode, that emits selective excitation wavelength.

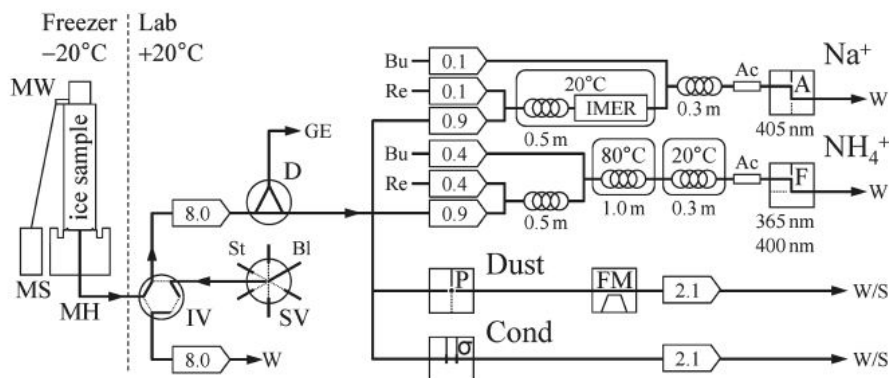


Figure 5: Setup of the Copenhagen CFA system with a melthead (MH), melting speed sensor (MS), melting weight (MW), injection valves (IV) and selection valves (SV) for standards (St) and blanks, debubbler (D), line to the gas extraction unit (GE), reagents (Re), buffers (Bu), waste lines (W) and optional discrete sampling lines (S), Accurel membrane debubblers (Ac), immobilised enzyme reactor (IMER), detectors for absorption (A), fluorescence (F), dust particle (P) and conductivity (σ) and a flow meter (FM). The flow rates of the peristaltic pump tubes (in ml/min), reaction coil lengths, temperatures and detector light wavelengths are given in the scheme. Taken from M. Bigler et al (2011) [15].

3.3.1 DYE-3 Measurement

The available ice core from the drilling site DYE-3 in Southern Greenland covers a depth interval from 1753.3 m to 1918.3m, where there is a break in the sample sequence between 1819.4 m and 1865.3 m. This sample sequence has been analysed in autumn 2019 using the CFA system, where only a few changes were made. An additional conductivity meter was installed in order to test if particles are filtered out by passing the micromodule and thereby effecting the conductivity measurement. Comparing the two records, this seems to be the case. However, the data detected by the conductivity meter, which was installed after the micromodule, are used for further analysis. A standard solution run was carried out before and after each run to achieve a reference point for the data measured in the ice core and to determine an individual time delay. A multielement standard solution covering the measurements of Na^+ , Ca^{2+} , NH_4^+ and the conductivity was used. The acidity signal reacted to two standard solutions (HCl and NaOH). The concentrations of the respective solutions had to be tuned for the different ice cores and climate periods during the analysis. Running MilliQ-water through the system twice a day controls the quality of the apparatus. The temperature of the melthead was mostly set to 50 °C, resulting in a rather constant melt speed of around 4 cm/min. The temperature was slightly raised when melting through an irregular break, increasing the melt speed, to avoid larger amounts of air entering the system. The meltwater for Bag 1704 to 1868 was sampled in a vial individually after running through the system. It can be used as backup data for subsequent discrete analysis. The measured concentrations were recorded as function of the acquisition time. Breaks in the ice sample, the beginning of a new bag, as well as the start and the end of each run were logged in the software program. Thus, they can be separated out of the record, since here the signal tends to be contaminated.

3.4 Annual Layer Counting

In the DYE-3 ice core annual layers are most distinctly visible in the dust and the conductivity signal. In order to estimate the annual layer thickness, this data, measured by the CFA system, is plotted against the acquisition time for each bag of approximately one meter length. Figure 4 contains a plot of the dust and the conductivity record from Bag 1741, showing an annual signal. Before the analysis, end surfaces and breaks are removed to de-contaminate the ice, resulting in missing data. Regular cuts at the end of a bag usually only account for a small lack of data, while at irregular breaks the ice sometimes has to be trimmed by cutting off a few centimetres. Therefore, some annual layers may be missing in the record. In this analysis the removed ice by the breaks is accounted for by using the length after preparing the ice as the whole bag length. The annual layer thickness is assumed to be constant over one bag, making the missing data negligible. Some breaks still can be contaminated at the surface, resulting in a high dust signal, which can be mistakenly interpreted as an annual signal. A peak in the dust signal due to contamination at a break around 4,000 s after the beginning of the run can be seen in Figure 4. Since the other records are not following the same trend, a volcanic signal can be ruled out. The annual peaks are counted in the two records separately. As can be seen in Figure 4, a lot more annual peaks are resolved in the dust than in the conductivity signal. Since the annual layer thickness in the analysed period is expected to be maximum 3 cm, the dust record is assumed to be the more reliable one. However, if there is a peak in conductivity, but the corresponding one in the dust signal is missing, it is included in the counting. In a period of constant climate conditions the layers are of approximately the same thickness, meaning that the annual peaks should occur with a constant frequency. Therefore, if an annual peak is expected based on the interpretation of the frequency, one can be counted even though it is not clearly visible in the record.

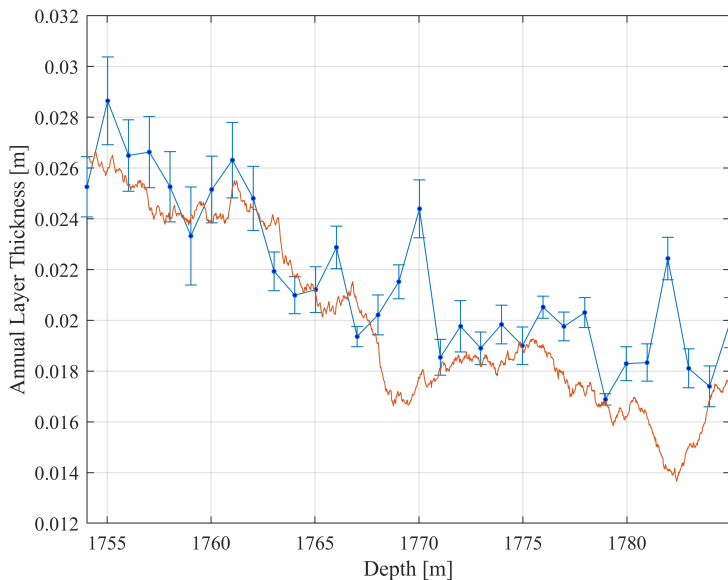


Figure 6: Plot of the annual layer thickness during the Holocene from the DYE-3 ice core in a depth interval from 1754m to 1785m. The blue curve shows the annual layer thickness based on the dust and conductivity signal, the red data is based on measurements of the DYE-3 ice core. Here annual layers were counted based on the stable water isotope signal. The uncertainties, included as errorbars, correspond to counted uncertain years.

Those 'uncertain annual layers' are counted as 0.5 ± 0.5 and amount to the accumulated error by summing them up. This so-called maximum counting error (MCE) thereby has the size of $N \times 0.5$ for N uncertain years [16]. Uncertainties on the measurement due to the apparatus used in CFA system as well as on the length of the bag has been neglected as they are relatively small compared to the MCE. When the number of annual layers for each bag is known, it is translated to the annual layer thickness by dividing the bag length by the number of counted peaks. The MCE has to be converted into an uncertainty on the annual layer thickness, which is done using the law of error propagation [17]. The annual layer thickness including their uncertainties are plotted as connected discrete values against depth in Figure 6. As reference the annual layer thickness determined 40 years ago are plotted as the red curve [18].

The annual layer counting focused on in this thesis is based on only two parameters, where the dust signal is decided to be the more reliable one. Every bag yields one discrete data point for every meter of ice. The reference graph instead is made from annual layer counting based on stable water isotopes [18]. The counts can not be considered to be unbiased, since new knowledge was gained during the counting process, changing the expectations and thereby influencing the next count. An increased melt speed when melting through breaks or gaps between two bags diminishes the depth resolution, causing not all the layers to be visible.

The depth interval from 1755 m to 1780 m covers the Holocene, a period of rather intermediate climate with higher accumulation rates and thereby thicker annual layers. The annual layers in preceding period with glacial climate conditions, the Younger Dryas, are concluded to be too thin to be visible in the record. The Younger Dryas lasted about 1,200 years (around 12,900 to 11,700 years before present) and is found in a depth of 1787 m to 1793 m, covering a piece of approximately 6.5 m ice. This corresponds to an annual layer thickness of about 5 mm. For the CFA system the time resolution of the conductivity measurement is 11 s [15], with an average melt speed of about 4 cm min^{-1} , the depth resolution is around 7 mm. Assuming the time resolution of the dust signal to be approximately of same size as for the other signals annual layers much thinner than 10 mm can not be detected.

3.5 Dansgaard-Johnsen Model

The thinning of the annual layers in an ice sheet can be described by a simple steady state model, the Dansgaard-Johnsen Model. This model allows the horizontal velocity to vary with depth and is based on several assumptions. Firstly, the surface and the bedrock are seen as perfectly horizontal. The total ice thickness, H , of the ice sheet is defined to be constant with time. Additionally, a mean annual accumulation rate is determined and held constant over the time period. The model can therefore only be used in periods of constant climate, like during the Holocene. The ice flow through the glacier is assumed to be plane [19]. The horizontal velocity, $u(x, z)$, illustrated in Figure 2 as V_x , is said to be constant with depth until some distance, h , above the bedrock, which is not varying with time either. Here x is defined as the distance from the ice divide along the flow line, and z as the distance above the bedrock. Below this depth the horizontal strain rate decreases linearly until the bedrock is reached. Here in the thin basal layer the shear deformation is fast and a basal sliding velocity, FB , is included. It can be seen in Equation 7, where it is expressed by a surface velocity constant in depth, $u_s(x)$.

$$u(x, z) = \begin{cases} u_s(x) & h \leq z \leq H \\ u_s(x) \frac{z}{h} & 0 \leq z < h \\ u_s(x) FB x & z = 0 \end{cases} \quad (7)$$

The surface velocity can be determined considering mass balance. The ice flux at x is

described as the vertically integrated horizontal velocity and can be seen in Equation 8.

$$Q = \int_0^H u(z) dz = \bar{u}H = u_s \left(H - \frac{1}{2}h(1 - FB) \right) \quad (8)$$

Here Q is the the total flux, H the ice thickness and the horizontal velocity is averaged over depth, indicated by \bar{u} . The flux has the dimensions of area per time. Considering the mass balance under the assumption of a constant accumulation rate along the flowline it follows:

$$\int_0^x a dx = ax = h\bar{u} \quad (9)$$

$$\Rightarrow u_s = \frac{a}{\left(H - \frac{1}{2}h(1 - FB) \right)} \quad (10)$$

Defining a constant $r = a/(h(H - \frac{1}{2}h(1 - FB)))$, the horizontal velocity can be expressed from Equation 7 as it is shown in Equation 11.

$$u(x, z) = \begin{cases} rhx & h \leq z \leq H \\ rhx \left(FB + (1 - FB) \frac{z}{h} \right) & 0 < z < h \\ rhx FB & 0 = z \end{cases} \quad (11)$$

Since the ice flow is assumed to be plane the continuity equation in Equation 12 is valid.

$$\frac{\partial u}{\partial x} + \frac{\partial w}{\partial z} = 0 \quad (12)$$

Consequently, the horizontal strain rate is equal to the negative vertical strain rate and by integrating the horizontal velocity, the vertical velocity of the ice flow, $w(z)$, is found and can be seen in Equation 13.

$$w(z) = \begin{cases} -rh \left(z - \frac{1}{2}h(1 - FB) \right) & h \leq z \leq H \\ -rh \left(FBz + \frac{1}{2}(1 - FB) \frac{z^2}{h} \right) & 0 < z < h \\ 0 & z = 0 \end{cases} \quad (13)$$

The model parameters are determined by fitting a linear regression to the data of the Holocene, where the climate is approximately constant. The intersection with the y-axis, $z(0)$, yields the value for h , as can be seen from Equation 14.

$$z(0) = \frac{1}{2}h(1 - FB) \quad (14)$$

The layers of equal age, called isochrones, will be horizontal as the vertical velocity is not dependent on x. At the surface, where $z = H$, the vertical velocity is equal to the negative accumulation, a . Maintaining steady state conditions each annual layer is replaced by the overlying new one and as the ice sinks with the vertical velocity, the annual layer thickness profile can be described using the same expressions. The plot in Figure 7 illustrates the gradually thinning of the layers, as the vertical velocity decreases linearly with depth, occurring during the Holocene. Changing climate conditions can be seen after a depth of about 1,500 m. The Dansgaard-Johnsen model was applied to the data of several ice cores in Greenland. However, the model could not be applied properly to the ice cores from Renland, Recap, Camp Century and DYE-3, as the layers within the last 10% of the core are too thin.

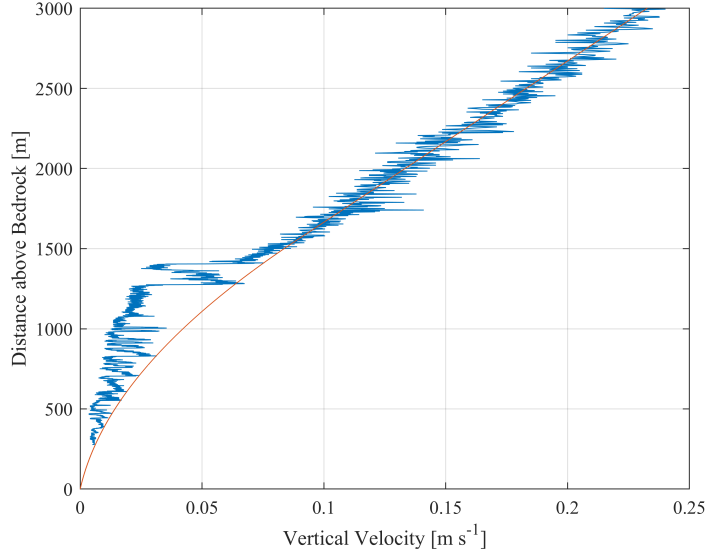


Figure 7: Plot of the vertical velocity through the GRIP ice core as function of the distance above the bedrock determined by use of the Dansgaard-Johnsen model. The modelled vertical velocity is illustrated by the red curve.

4 Accumulation Rate

The past accumulation rates can be dated by use of the Dansgaard-Johnsen Model, in which the accumulation rate now is allowed to change with time. From this model the total thinning of the determined annual layers can be calculated. Using the thinning rates the accumulation rates can be reconstructed, as it is proportional to the vertical strain rate, $\frac{\partial v}{\partial y}$, and therefore changes in time as well. The friction at the bedrock, FB , and the model parameter h remain constant, and the total ice thickness is assumed to be unchanged, so that only the slope of the linear function varies. Under assumption that the shape function is unaltered, the accumulation rate can be calculated using the expression in Equation 15.

$$A(z) = \frac{\lambda(z)}{Th(z)} \quad (15)$$

Here $A(z)$ is the accumulation rate, $\lambda(z)$ the annual layer thickness and $Th(z)$ the thinning function. All variables are dependent on the height above the bedrock, z . That way the accumulation rate is transferable to the glacial time, even though it is deduced from a model valid for steady state conditions only. The accumulation rate can be related to the temperature, as warmer air masses tend to contain more moisture than colder air masses.

4.1 Accumulation Rate and Stable Water Isotopes

Both the amount of stable water isotopes in ice and the accumulation rate can be linked to past climate conditions. The annual mean amount of stable water isotopes has been proved to be clearly correlated to the annual mean temperature. The relation, presented in Equation 16, was found empirically by Johnsen et al. (1989) and is applicable to the Greenland ice sheet, where it needs to be tuned in order to match the different drilling sites [20].

$$\delta^{18}O = 0.67T - 13.7 \quad (16)$$

Here $\delta^{18}O$ is given in ‰ and the temperature, T , is in °C. Since this relation is linear, $\delta^{18}O$ can be compared directly to the accumulation rate. Low values of $\delta^{18}O$ represent cold climate and correspond to low accumulation rates, higher $\delta^{18}O$ -values correspond to higher accumulation and represent a warmer climate. Empirically determined relationships between temperatures and accumulation rates can support this hypothesis of an increase in accumulation rate with rising temperatures. An exponential relationship between the accumulation rate and $\delta^{18}O$ has been found [21]. It is presented in Equation 17.

$$A(t) = A(0) \exp(c_1 (\delta^{18}O + c_2)), \quad (17)$$

$A(0)$ is the current ice equivalent accumulation rate. The expression needs to be tuned for the several drilling sites by varying the constants, c_1 and c_2 . This relationship is presented for data from ice cores from GRIP, GISP2, NGRIP and NEEM in Figure 8.

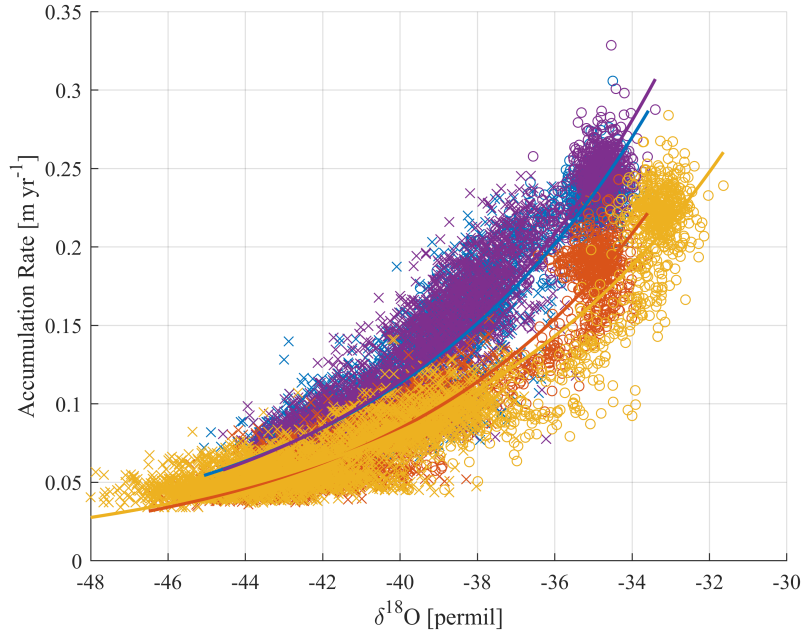


Figure 8: Plot of the accumulation rates versus $\delta^{18}O$ for the drilling sites GRIP (blue), GISP2 (purple), NGRIP (red) and NEEM (yellow). The least square exponential fits are plotted in the corresponding colour. The accumulation rates during the interglacial are marked by o and the rates during the glacial period are marked by x.

4.2 Sensitivity of the Accumulation Rate to Changes in $\delta^{18}O$

How the accumulation rate responds to changes in $\delta^{18}O$ can be described by the constant, c_1 , which can be found by differentiating the exponential function in Equation 17. A least square exponential fit to the data (Figure 8) yields values of this parameter for the four ice cores, presented in Table 1.

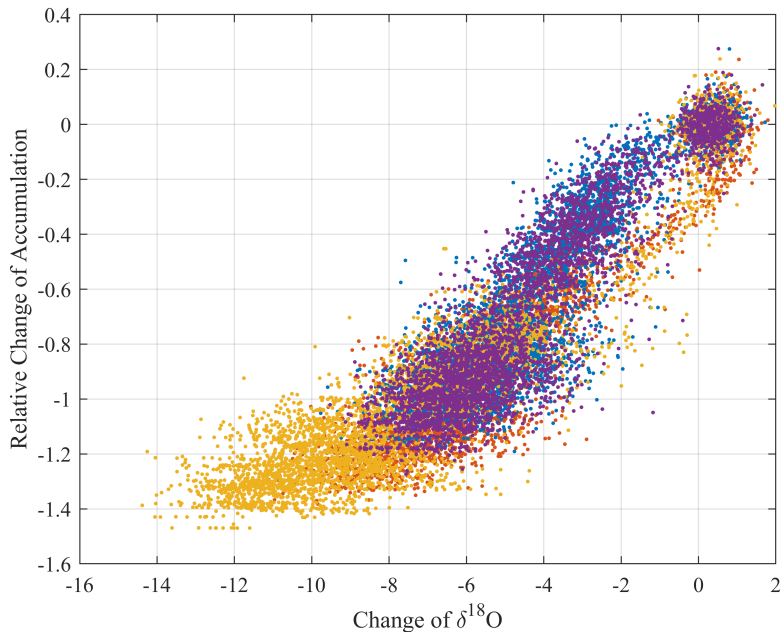


Figure 9: Plot of the relative accumulation rate compared to an average of the last 1,000 years versus the difference in $\delta^{18}\text{O}$ compared to an average of the last 1,000 years for the drilling sites GRIP (blue), GISP2 (purple), NGRIP (red) and NEEM (yellow) over the whole record, including both the glacial and the interglacial.

	$\frac{1}{A} \frac{\partial A}{\partial \delta^{18}\text{O}}$ [% ‰ ⁻¹]
GRIP	14.5 ± 0.1
GISP2	14.92 ± 0.07
NGRIP	15.08 ± 0.09
NEEM	13.7 ± 0.1

Table 1: Values of the sensitivity of the accumulation, A , rate to changes in $\delta^{18}\text{O}$ in percent per permille. The uncertainties are determined by the standard deviation on the fitting parameters.

From this it can be seen, that the sensitivity of the accumulation rate to changes in $\delta^{18}\text{O}$ only show small fluctuations over Greenland. The relative change in accumulation rate compared to an average of the last 1,000 years, $\overline{A_{1000}}$, is found to be linearly dependent on the temperature:

$$\frac{\Delta A}{A} = c_1 \Delta \delta^{18}\text{O} \quad (18)$$

Since c_1 is nearly constant for the different drilling sites, variations in $\delta^{18}\text{O}$ are crucial. From Figure 9 it can be seen, that this applies for both the Holocene as well as all DO events during the glacial. Here changes in the accumulation rate are defined as $\Delta A = \frac{A - \overline{A_{1000}}}{\frac{1}{2}(A - \overline{A_{1000}})}$ and plotted against the difference in $\delta^{18}\text{O}$ compared to an average value of the last 1,000 years before present. The correlation can be seen to be linear and almost constant for the drilling sites.

5 Investigation of the Dansgaard-Oeschger Events

The accumulation rates from each site, derived by the use of the Dansgaard-Johnsen Model, are plotted against the age of the ice in years before present (later denoted as years b2k). For comparison $\delta^{18}\text{O}$ is plotted on the same timescale. The records of GRIP, GISP2 and NEEM cover the past 80,000 years, whereby the data resolution of the latter accumulation record is lower in the first 20,000 years. The data from the NGRIP ice core only cover the last 60,000 years. Both records can be seen in Figure 10. The sites GRIP and GISP2 are located in Central Greenland on the ice ridge and east from the divide, respectively, only 28 km apart. Here the ice sheet is at its highest elevation. NGRIP and NEEM are both situated on the ice ridges 314 km and 679 km, respectively, north from the summit. The Greenlandic ice sheet shows a north-going decrease of elevation. The locations of the drilling sites can be seen in Figure 13.

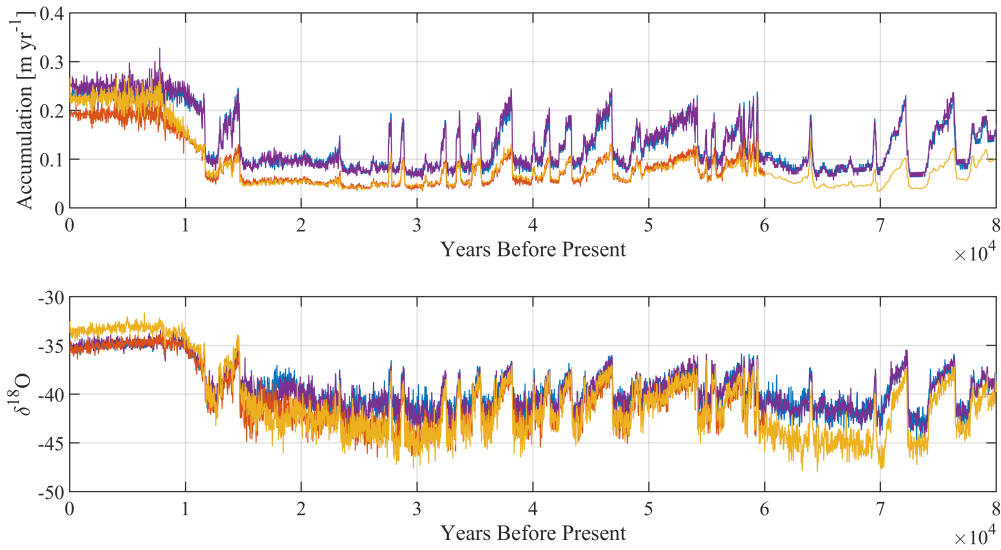


Figure 10: a) Plot of the accumulation rate as a function of the age of the ice in years for the drilling sites GRIP (blue), GISP2 (purple), NGRIP (red) and NEEM (yellow). b) Plot of $\delta^{18}\text{O}$ as a function of the age of the ice in years for the drilling sites GRIP (blue), GISP2 (purple), NGRIP (red) and NEEM (yellow).

The first 11,700 years of the record represent the Holocene. During the last 8,000 years, both data sets show only small fluctuations as the climate was rather unchanged. Abrupt shifts to higher values during the last glacial in both records indicate the DO events, which occurred equally in whole Greenland. The data from GRIP and GISP2 show almost equal values throughout the whole record, since they are in such short distance to each other. Similarly, the records for NGRIP and NEEM do not differ a lot from each other, since they are situated close to each other when comparing the distance to the other two drilling sites. In the last interglacial (up to 8,000 years b2k) it is conspicuous, that the NEEM record shows higher values of $\delta^{18}\text{O}$, indicating higher temperatures, while the accumulation rate is lower than for GRIP and GISP2. This indicates, that even though the precipitation is strongly correlated to the temperature it also depends on the wind direction and more complex weather systems. As a result, the precipitation is not uniformly distributed over Greenland. The accumulation rate for Greenland is presented in Figure 13.

5.1 Relative Changes in Accumulation Rate and $\delta^{18}\text{O}$

Because of the irregular distribution of the precipitation, the relative change of the accumulation rate compared to the averaged accumulation of the last 1,000 years is calculated in order to examine, how the accumulation rate has changed during periods of different climate conditions. Therefore, the accumulation as function of time is divided by the average value of the accumulation of the last 1,000 years and expressed in percent. Consequently, the accumulation rate of the past 1,000 years is a 100%, and is expected to be less in glacial periods. The accumulation rate is presented for the four drilling sites as function of time in Figure 11. Considering the glacial, it can be seen from the curves, that the relative change in accumulation rate increases with increasing distance to the summit of the ice sheet. The accumulation at NEEM is decreased with about 80% whereas on top of the ice sheet at the sites in Central Greenland it only is about 65% less than during the last 1,000 years. The trend pertains to the stadials as well as to the interstadials. The difference in the relative change between the drilling sites is more striking when the climate changes abruptly, like at the onset of the stadials or the interglacial. In the period of 12,7ka to 8ka b2k, the accumulation rate for GRIP and GISP2 is smaller than for NGRIP and NEEM. It is noteworthy, that the summit ice cores reach the current mean value in year 10ka b2k, while NGRIP and NEEM undergo further changes until 8ka b2k.

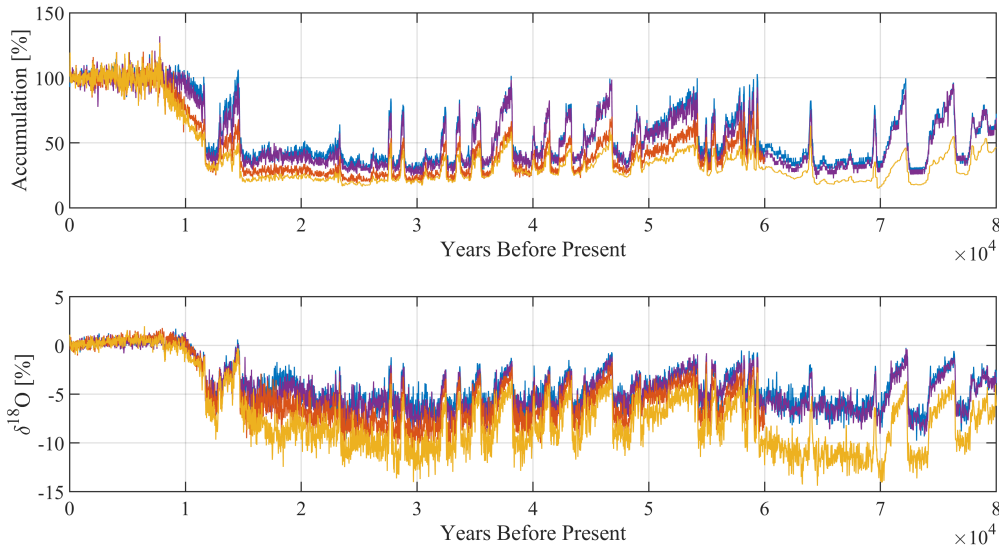


Figure 11: Plot of the percentage relative change in the accumulation rate and the change in $\delta^{18}\text{O}$ as a function of years before present for the drilling sites GRIP (blue), GISP2 (purple), NGRIP (red) and NEEM (yellow).

As explained in Section 4.1, the changes in the accumulation rate can be explained by changes in temperature, and thus changes in $\delta^{18}\text{O}$. Since the fluctuations in the accumulation rate portend to be site-specific, variations in the $\delta^{18}\text{O}$ record of the different drilling sites are expected. In order to study this dependency, the difference between $\delta^{18}\text{O}$ and the average over the last 1,000 years is plotted against the time for the different drilling sites in Figure 11. Hence, $\delta^{18}\text{O}$ for all the ice cores shows values around zero during the last 8,000 years before present, and is increasing when considering the glacial from 12,7ka b2k. The $\delta^{18}\text{O}$ -values are following the same trend as the accumulation rate, in which the deviation from the mean value is increasing with distance northward from the centre of the ice sheet.

5.2 Correlation to Elevation Changes

The shift in the $\delta^{18}\text{O}$ -values is suspected to be correlated to the location of the drilling sites on the ice sheet. As the decline tends to increase with northward direction from the ice summit, the $\delta^{18}\text{O}$ records of NGRIP and NEEM compared to the average of the summit ice cores are plotted in Figure 12 as the red and yellow curve, respectively. The dashed and the dotted line illustrate the corresponding mean values of each record. For NGRIP the value of $\delta^{18}\text{O}$ was about 2‰ less compared to the value measured in the summit ice cores and relative to the interglacial value. Moving further north to the NEEM drilling site, the relative change increases to 3-4 ‰. The DO events are slightly visible in both curves, but do not seem to be decisive for fluctuations in the climate signal. From this it can be concluded, that the shift in $\delta^{18}\text{O}$ is not only due to general climate fluctuations in Greenland, but have to be correlated to the drilling site.

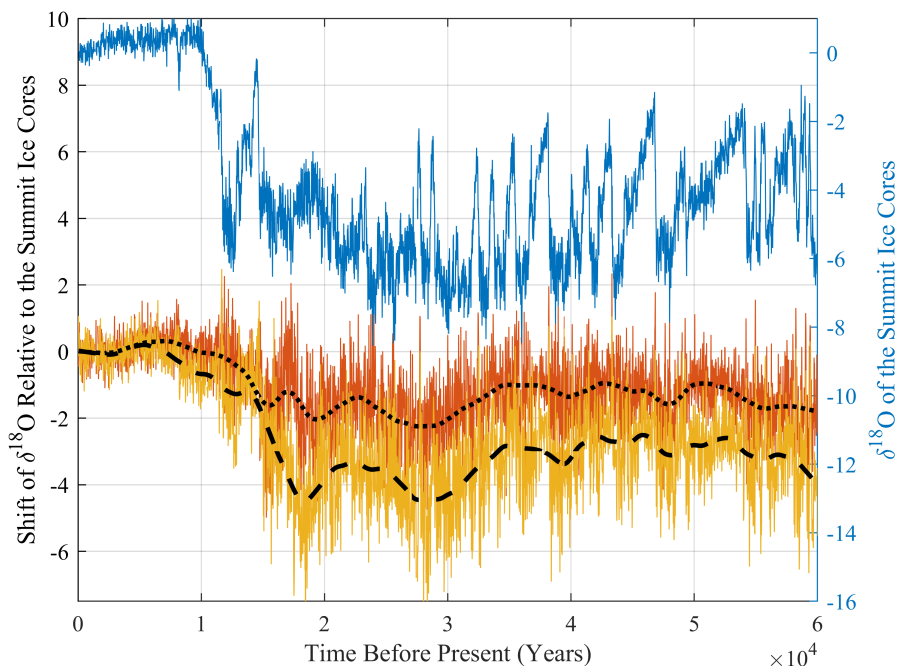


Figure 12: Plot of $\delta^{18}\text{O}$ as function of time in years before present. The blue curve shows the average value of the summit ice cores, GRIP and GISP2. The red and the yellow curves represent the shift of $\delta^{18}\text{O}$ relative to the summit ice cores for NGRIP and NEEM, respectively. All records are compared to an average of the last 1,000 years. The dotted and the dashed line are the mean value of the records.

Vinther et al. (2009) found a correlation between the stable water isotopes and the elevation of the ice on the basis of height, temperature and $\delta^{18}\text{O}$ data of the Holocene taken from several drilling sites in Greenland. A shift in $\delta^{18}\text{O}$ of 0.6‰/100m height has been determined [22]. Accordingly, the accumulation rate can be considered a function of both climate and elevation. Assuming the climate distribution to be uniform in Greenland, locally varying $\delta^{18}\text{O}$ -values might be related to the changing shape of the ice sheet during the glacial and again after the onset of the Holocene. The current elevation distribution of parts of the Greenland ice sheet can be seen in Figure 13. Due to the parabolic shape of an ice sheet the elevation decreases with increasing distance to the summit. According to investigations of the Greenland moraine

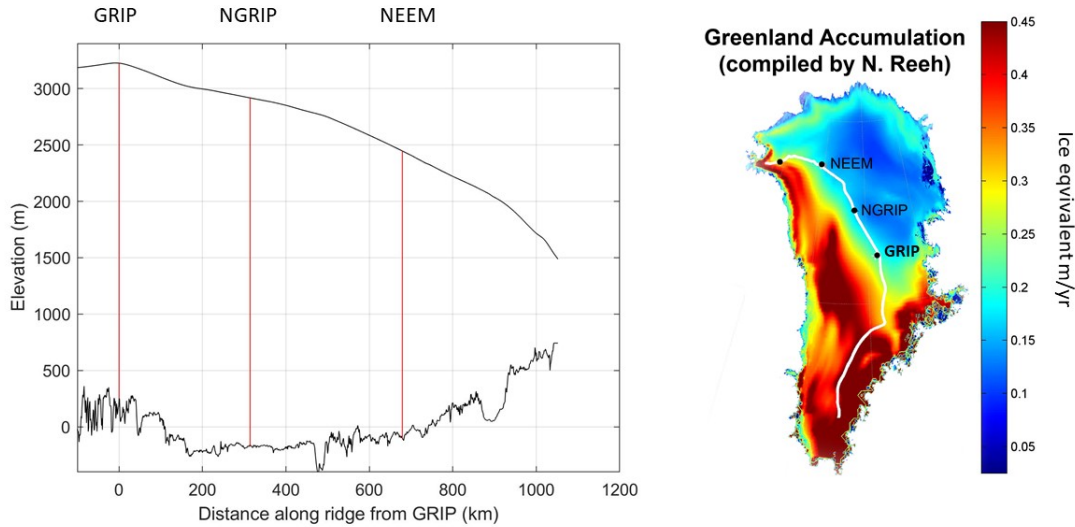


Figure 13: Plot of the elevation distribution of the Greenland ice sheet northward from the summit. The lower curve represents the ground elevation under the ice sheet and the upper curve the surface elevation. The red lines indicate the total ice thickness of the drilling sites GRIP, NGRIP and NEEM. The white line on the accumulation map of Greenland indicates the ice ridge, including the drilling sites.

the ice sheet is expected to have been longer during the last glacial. It might even have fused with the ice sheet still present in North American. Due to the gravity influenced flow of the ice, an ice sheet always will maintain its parabolic shape (Figure 2]. Thus, the elevation change will be most pronounced the more distant from the centre of the ice sheet. The temperatures in general, can be said to be lower at higher elevation, which corresponds to a lower value of $\delta^{18}\text{O}$. Applying the relation by Vinther et al. (2009) the shift of 2‰ observed in the NGRIP ice core corresponds to a change of 300m. The elevation at the NEEM drilling site is expected to have been up to 600m higher during the last glacial maximum.

6 Conclusion

Based on ice core records, including depth, age and $\delta^{18}\text{O}$ data from several drilling sites in Greenland the change in accumulation with temperature over the last 60,000 years before present was studied. Applying the Dansgaard-Johnsen flow model the accumulation rate at GRIP, GISP2, NGRIP and NEEM was determined. Comparing this record to the $\delta^{18}\text{O}$ -values an intimate coherence between the accumulation rate and the temperature, represented by $\delta^{18}\text{O}$, has been proven. The sensitivity of the accumulation rate to changes in $\delta^{18}\text{O}$ is almost constant for the different drilling sites and can be applied to the interglacial period as well as during the Dansgaard-Oeschger events in the last glacial. Considering the relative changes compared to an average value over the past 1,000 years in both accumulation rate and $\delta^{18}\text{O}$, the ice sheet can be supposed to have changed in shape during the last glacial maximum. While the ice thickness on the ice ridge is expected to have been almost invariant, the elevation

increased with increasing distance from the summit. This might explain the relative shift in $\delta^{18}\text{O}$ observed in the NGRIP and NEEM ice cores, as the temperature tends to decrease with higher elevation. Hence, lower values of $\delta^{18}\text{O}$ can be found in these ice cores. Applying a relation between changes in $\delta^{18}\text{O}$ and changes in height, developed by Vinther et al. (2009), the ice thickness at the present location of the drilling site NEEM has decreased by 600m since the last glacial maximum, while the drilling site NGRIP has decreased by about 300m. With increasing temperatures the Greenlandic ice sheet can be expected to maintain its height around the ice ridge in the interior, whereas its volume will decrease towards the ice margins. This is a rather uncertain hypothesis, since the applied relationship has been calibrated for the current climate period and might not be applicable to glacial periods. In that case, the more northern locations of the drilling sites leading to a decrease in temperature could be considered a possible interpretation of the $\delta^{18}\text{O}$ fluctuations.

7 References

- [1] Sea level. <https://climate.nasa.gov/vital-signs/sea-level/>. Accessed on January 7, 2020.
- [2] State of the cryosphere. is the cryosphere sending signals about climate change. https://nsidc.org/cryosphere/sotc/sea_level.html. Accessed on January 7, 2020.
- [3] D. et al. Dahl-Jensen. *The Greenland Ice Sheet in a Changing Climate. In: Snow, Water, Ice and Permafrost in the Arctic (SWIPA)*. Arctic Monitoring and Assessment Programme (AMAP), 2017.
- [4] S. Rasmussen et al. A stratigraphic framework for abrupt climatic changes during the last glacial period based on three synchronized greenland ice-core records: Refining and extending the intimate event stratigraphy. *Quaternary Science Reviews*, 106, 11 2014.
- [5] H. Braun. Strong indications for nonlinear dynamics during dansgaard-oeschger events. *Climate of the Past Discussions*, 5, 07 2009.
- [6] B. J. R. Bizet. High resolution analysis of the northgrip ice core microstructures and fabrics: A detailed study of the dansgaard-oeschger events 1, 8 and 19. June 12, 2006.
- [7] The firn zone: Transforming snow to ice. http://www.iceandclimate.nbi.ku.dk/research/drill_analysing/cutting_and_analysing_ice_cores/analysing_gasses/firn_zone/. Accessed on January 11, 2020.
- [8] K.M. Cuffey and W.S.B. Patterson. *The Physics of Glaciers*. Butterworth-Heinemann.
- [9] Raymond S. Bradley. *Paleoclimatology*. Academic Press, third edition, 2015.
- [10] International Atomic Energy Agency, Scientific United Nations Educational, and Cultural Organization. *Environmental Isotopes in the Hydrological Cycle - Principles and Applications*, March 2000.
- [11] Reference sheet for international measurement standards. https://nucleus.iaea.org/rpst/documents/VSMOW_SLAP.pdf. Accessed on November 27, 2019.
- [12] W. Dansgaard et al. One thousand centuries of climatic record from camp century on the greenland ice sheet. *Science (New York, N.Y.)*, 166:377–80, 11 1969.

- [13] Tephra und pyroklastika. [http://www.vulkane.net/vulkanismus/tephra-pyroklastika.html#:~:targetText=Die%20Tephra%20wird%20nach%20ihrer,B1%C3%B6cke%20\(gr%C3%B6%C3%9Fer%2064%20mm\)](http://www.vulkane.net/vulkanismus/tephra-pyroklastika.html#:~:targetText=Die%20Tephra%20wird%20nach%20ihrer,B1%C3%B6cke%20(gr%C3%B6%C3%9Fer%2064%20mm)). Accessed on November 16, 2019.
- [14] Ice core impurities of volcanic origin. http://www.iceandclimate.nbi.ku.dk/research/past_atmos/ice_core_impurities/impurities_volcanic_origin/#:~:targetText=In%20ice%20cores%2C%20volcanic%20layers,mainly%20sulphate%20and%20sometimes%20fluoride. Accessed on November 16, 2019.
- [15] M. Bigler et al. Optimization of high-resolution continuous flow analysis for transient climate signals in ice cores. *Environmental Science & Technology*, 45:4483–9, May 2011.
- [16] K. Andersen et al. The greenland ice core chronology 2005, 15-42 ka. part 1: constructing the time scale. *AGU Fall Meeting Abstracts*, 12 2006.
- [17] J. R. Taylor. *An Introduction to Error Analysis - Reconstructing Climate of the Quaternary*. University Science Books, second edition, 1982.
- [18] B. Vinther et al. Synchronized dating of three greenland ice cores throughout the holocene. *Journal of Geophysical Research*, 111, 07 2006.
- [19] D. Dahl-Jensen et al. Past accumulation rates derived from observed annual layers in the grip ice core from summit, central greenland. *Peltier W.R. (eds) Ice in the Climate System. NATO ASI Series (Series I: Global Environmental Change)*, 12, 1993.
- [20] S.J. Johnsen et al. The origin of arctic precipitation under present and glaciation conditions. *Tellus*, pages 452–468, 01 1992.
- [21] S. Buchardt. Investigating the past and recent 18o-accumulation relationship seen in greenland ice cores. *Climate of the Past*, 8:2053–2059, 12 2012.
- [22] B. Vinther et al. Holocene thinning of the greenland ice sheet. *Nature*, 461:385–8, 09 2009.